Available online at www.sciencedirect.com

ScienceDirect

Publishing Services by Elsevier

International Journal of Naval Architecture and Ocean Engineering 10 (2018) 529–544
http://www.journals.elsevier.com/international-journal-of-naval-architecture-and-ocean-engineering/

Development of a safe operation capability chart as the design basis of a rudder area

Youngjun You [a,*], Sewon Kim [a], Woojin Kim [b]

[a] *Daewoo Shipbuilding and Marine Engineering Co., LTD. (DSME), South Korea*
[b] *Hyundai Heavy Industries (HHI), South Korea*

Received 21 February 2017; revised 2 August 2017; accepted 13 September 2017
Available online 6 November 2017

Abstract

Ship owners now demand a new design approach for the rudder that considers detailed design information such as maneuverability and environmental loads etc. on a quantified basis. In this paper, we developed the concept of a safe operation capability chart for the design of a rudder area. The chart can be used as the basis of design considering the maneuverability and environmental loads. To confirm the applicability of the safe operation capability chart for use as the basis of design, four different rudders are assumed in this work. First, it is determined whether or not it is appropriate to design a rudder by applying a conventional design approach based on IMO maneuvering tests. The proposed concept is reviewed for use as the basis of the design by investigating the effect of rudder area on capability charts that are plotted according to the rudder under various environmental conditions.

Keywords: Maneuverability; Environmental loads; Safe operation capability chart; Design; Rudder

1. Introduction

In shipbuilding companies in South Korea, large ships such as container ships, Liquefied Natural Gas Carriers (LNGCs), and Very Large Crude oil Carriers (VLCCs) have mostly been constructed. They are generally operated based on a simplified navigation plan that minimizes complicated maneuvering motions in terms of sailing safety. Accordingly, the hull, propeller, and rudder are designed by considering mandatory scenarios such as course changing, turning, and stopping, etc.

The designs are confirmed by conducting mandatory tests to evaluate the maneuverability of the ship based on the recommendation proposed by the International Maritime Organization (IMO) (IMO, 2002). These tests include an initial turning test, a 35° turning test, a 10°/10° zigzag test, a 20°/20° zigzag test, and a stopping test at design speed. The obtained values from each test are then compared with the criteria regulated in the regulation.

To evaluate the maneuverability of the ship, simulations, model tests, and sea trials for the mandatory tests have been used (Kim et al., 2006, 2009, 2001). Because model tests can be conducted after the initial design of a ship and sea trials can be performed after a ship has launched, simulations are frequently used to evaluate the maneuverability of a designed ship from an initial design stage. Hydrodynamic coefficients for a hull, which are needed to simulate the maneuvering behavior of a ship, have been obtained from empirical formulas (Kijima et al., 1990). Recently, a new approach has been presented to obtain the coefficients by conducting virtual captive model tests using Computational Fluid Dynamics (CFD) (Sung and Park, 2015).

A rudder is designed by using empirical formulas proposed by classifications such as the Germanischer Lloyd (GL) and the International Association of Classification Societies (IACS) to determine the rudder area and the capacity of the

* Corresponding author.
E-mail address: marineryou@gmail.com (Y. You).
Peer review under responsibility of Society of Naval Architects of Korea.

https://doi.org/10.1016/j.ijnaoe.2017.09.006

steering gear (Germanischer Lloyd (GL), 2013; IACS, 1990). Although this design approach has been used for several decades, when building new ships, ship owners demand that the rudder design considers detailed design information such as resistance, maneuverability, torque, and environmental loads, etc. on a quantified basis. However, a method for designing the rudder as requested is not yet available, and a new approach is needed to design a rudder by considering the prescribed factors to meet the needs of ship owners.

Similarly, a request has recently been made to design a rudder considering the environmental effect in the Suez Canal (You and Kim, 2016). Basic research was conducted to assess the appropriateness of the designed rudder. Before a design methodology of a rudder is determined, a quantifying method of sailing safety is needed that considers maneuverability and environmental loads such as wind and current. Such as the method was recently proposed (You et al., 2017).

The suggested approaches (You and Kim, 2016; You et al., 2017) overlap the latest research trends. Recently, discussions on applying the Energy Efficiency Design Index (EEDI) have been carried out by the IMO (Jung, 2011), and the regulations of the International Organization for Standardization (ISO) have been updated to consider the environmental effects, including wind, waves, current, water depth, etc., to predict the speed from a sea trial (International Organization for Standardization (ISO) 15016, 2015). Nowadays, EU funded research project called as the Energy Efficient Safe Ship Operation (SHOPERA) (Papanikolaou, Zaraphonitis, Bitner-Gregersen, Shigunov, Moctar, Soares, Reddy, Sprenger). To consider energy efficiency on ship design, the relation between environmental loads and operating performance including CO_2 emission, minimum powering, and maneuvering has been studied (Prpic-Orsic et al., 2016; Papanikolaou and Shigunov, 2014; Sutulo and Soares, 2015, 2016).

In this paper, we developed the concept of a safe operation capability chart for the design of a rudder. The chart can be used as the basis of design by considering detailed design information such as maneuverability and environmental loads.

First, this research is carried out on a twin-screw container ship while considering recent market trends. To simulate the maneuvering behavior of a ship, the hydrodynamic coefficients for a hull and the lift coefficient of a rudder are mostly predicted from empirical formulas (Kijima et al., 1990; Fujii and Tsuda, 1961, 1962). Coefficients for resistance and thrust are obtained from model tests conducted by the Daewoo Shipbuilding and Marine Engineering Co., LTD. (DSME). Simulations are conducted by using a verified mathematical model (Kijima et al., 1990; You et al., 2017).

Environmental loads such as wind, wave and current are additionally considered. Wind load coefficients are obtained from empirical formulas and irregular wind speeds are generated from a wind spectrum (Fujiwara et al., 2001; Andersen and Løvseth, 1992). Wave loads are calculated by following the procedure process summarized in references (International Organization for Standardization (ISO) 15016, 2015; International Towing Tank Conference (ITTC), 2011). Wave drift forces and moment are calculated using the commercial software that called HYDROSTAR provided by Bureau Veritas (BV) classification. The relative speed of a ship under a given current is used to predict the hydrodynamic loads including the current loads (Hwang, 1980).

In the previous study, the concept of a safe operation judgment chart as a quantifying method of sailing safety was proposed, after maneuvering simulations were conducted under given operating conditions (You et al., 2017). The concept of the above mentioned chart was that sailing safety was quantified as a value from the calculated minimum relative distances between four edges of a ship and allowable safe boundaries by assuming a sailing ship with an autopilot system (Hasegawa and Kouzuki, 1987).

Here, the quantified concept of the safe operation judgment chart is developed as a safe operation capability chart. Fundamentally, the simulations are conducted identically. However, they are repeatedly conducted under different wind, wave, and current speeds at regular intervals. After the maximum wind speeds for safe operation are confirmed according to each wind direction, the searched values are marked on a polar plot. The envelope is called a safe operation capability chart.

This concept is similar to a Dynamic Positioning (DP) capability chart, where a radius axis indicates the tested wind speed and an angle axis indicates the tested wind direction (Hendzik, 2013). A DP capability chart has two purposes. First, a capability chart is used as the basis of design to determine the capacity of the equipped devices on a quantified basis. Second, an operating instruction can be guided for an operator to perform work safely. It is anticipated that the suggested safe operation capability chart can also be used to accomplish prescribed objectives. Like DP capability chart, polar capability charts are used to indicate the performance of a ship, as well (Prpic-Orsic et al., 2016; Papanikolaou and Shigunov, 2014).

To confirm the applicability of the safe operation capability chart for use as the basis of design, four different rudders are assumed. These rudders have different areas, although their aspect ratios are identical. It is determined whether or not it is appropriate to design a rudder by applying a conventional design approach based on IMO maneuvering tests. From the simulated results, determining the correct rudder area causes ambiguity, because all values meet the IMO maneuvering criteria related to the IMO maneuvering tests, and the differences between values are insignificant. In addition, effect of rudder area on capability charts which are plotted according to rudders under various environmental conditions is investigated to determine whether the proposed concept can be used as the basis of design. Finally, the applicability of the suggested concept for use as the basis of design is confirmed to determine the rudder area.

2. Model ship and maneuvering equations of motion

2.1. Model ship and coordinate system

The twin-screw container ship that was studied in the previous research is also used here. The ship's specifications are briefly as follows: *Lpp* is 375.0 m, B is 59.0 m, T is 16.0 m, C_B is about 0.71, and A_R is 60.0 m^2.

Fig. 1 shows the coordinate system of this research. x_g and y_g indicate the global coordinate axis and δ_{PORT} and δ_{STBD} are the deflected angle of a rudder on the port and starboard side, respectively. U refers to the ship speed and Ψ is the heading angle of the ship.

2.2. Maneuvering equations of motion

Maneuvering equations of motion are shown in Eq. (1). m indicates the mass of the ship and I_{zz} refers to the mass moment of inertia. u and v are the longitudinal and transverse speeds, respectively, and r is the angular velocity (or turn rate). $\dot{u}$ and $\dot{v}$ indicate the time derivatives of longitudinal and transverse speed, respectively, and $\dot{r}$ is the time derivative of angular velocity. X and Y are the longitudinal and transverse forces acting on the ship, respectively, and N is the yaw moment.

$$\begin{aligned} m(\dot{u} - vr - x_G r^2) &= X \\ m(\dot{v} + ur + x_G \dot{r}) &= Y \\ I_{zz}\dot{r} + mx_G(\dot{v} + ru) &= N \end{aligned} \tag{1}$$

The forces and moment acting on the ship can be expressed as Eq. (2). The subscripts "H", "P", "R", "C", "WI" and "WA" indicate the hydrodynamic loads due to the hull, propellers, rudders, current, wind, and wave respectively. Ψ_C, Ψ_{WI}, and Ψ_{WA} are incident angles of the current, wind, and wave respectively. Because the effect of current is considered in hydrodynamic loads acting on the hull, "C" is added to "H" (Hwang, 1980).

$$\begin{aligned} X &= (X_H)_C + X_P + X_R + X_{WI} + X_{WA} \\ Y &= (Y_H)_C + Y_R + Y_{WI} + Y_{WA} \\ N &= (N_H)_C + N_P + N_R + N_{WI} + N_{WA} \end{aligned} \tag{2}$$

2.2.1. Hydrodynamic loads due to hull, propeller and rudder

Hull hydrodynamic loads are calculated as shown in Eq. (3). Many hydrodynamic coefficients such as added mass, added mass moment of inertia, and rudder lift coefficients can be predicted using empirical formulas (Kijima et al., 1990; Fujii and Tsuda, 1961, 1962). m_x and m_y indicate the added mass along the longitudinal and transverse directions. J_{zz} is the added mass moment of inertia and T is the draft of the ship. x_G indicates the *LCG* as defined in Table 1 and ρ is the density of sea water. An inverted comma (') indicates a non-dimensionalized value. Definitions of each hydrodynamic derivative and non-dimensionalization are identical to those in the previous research proposed by Kijima et al. (1990). However, the slopes and constants related to Y'_{vvr}, N'_{rr}, N'_{vrr} are slightly modified to match the simulated results with free running model test results (You et al., 2017).

$$X_H = -m_x\dot{u} + (m_y + X_{vr})vr + \left(\frac{1}{2}\rho \cdot L_{pp} \cdot T \cdot U^2\right) \cdot X_{uu}\cos^2\beta$$

$$Y_H = -m_y\dot{v} + m_x ur + Y_H(v', r')$$

$$N_H = -J_{zz}\dot{r} + N_H(v', r') + x_G \cdot Y_H(v', r')$$

where,

$$Y_H(v', r') = \left(\frac{1}{2}\rho \cdot L_{pp} \cdot T \cdot U^2\right) \cdot \left(Y'_v \cdot v' + Y_r \cdot r' + Y'_{vv} \cdot v'|v'| + Y'_{rr} \cdot r'|r'| + Y'_{vvr} \cdot v'v'r' + Y'_{vrr} \cdot v'r'r'\right)$$

$$N_H(v', r') = \left(\frac{1}{2}\rho \cdot L_{pp}^2 \cdot T \cdot U^2\right) \cdot \left(N'_v \cdot v' + N_r \cdot r' + N'_{vv} \cdot v'|v'| + N'_{rr} \cdot r'|r'| + N'_{vvr} \cdot v'v'r' + N'_{vrr} \cdot v'r'r'\right) \tag{3}$$

$$\beta = \frac{-v}{\sqrt{u^2 + v^2}}, \quad v' = v/U, \quad r' = r \cdot L_{pp}/U$$

$$X_{vr} = \frac{1}{2}\cdot\frac{\partial^2 X}{\partial v \partial r}, \quad X_{uu} = \frac{1}{2}\cdot\frac{\partial^2 X}{\partial u \partial u}, \quad Y_v = \frac{\partial Y}{\partial v}, \quad Y_r = \frac{\partial Y}{\partial r}, \quad Y_{vv} = \frac{1}{2}\cdot\frac{\partial^2 Y}{\partial^2 v}, \quad Y_{rr} = \frac{1}{2}\cdot\frac{\partial^2 Y}{\partial^2 r}, \quad Y_{vvr} = \frac{1}{6}\cdot\frac{\partial^3 Y}{\partial^2 v \partial r}, \quad Y_{vrr} = \frac{1}{6}\cdot\frac{\partial^3 Y}{\partial v \partial^2 r}$$

$$N_v = \frac{\partial N}{\partial v}, \quad N_r = \frac{\partial N}{\partial r}, \quad N_{vv} = \frac{1}{2}\cdot\frac{\partial^2 N}{\partial^2 v}, \quad N_{rr} = \frac{1}{2}\cdot\frac{\partial^2 N}{\partial^2 r}, \quad N_{vvr} = \frac{1}{6}\cdot\frac{\partial^3 N}{\partial^2 v \partial r}, \quad N_{vrr} = \frac{1}{6}\cdot\frac{\partial^3 N}{\partial v \partial^2 r}$$

$$X' = \frac{X}{\frac{1}{2}\rho \cdot L_{pp} \cdot T \cdot U^2}, \quad Y' = \frac{Y}{\frac{1}{2}\rho \cdot L_{pp} \cdot T \cdot U^2}, \quad N' = \frac{N}{\frac{1}{2}\rho \cdot L_{pp}^2 \cdot T \cdot U^2}$$

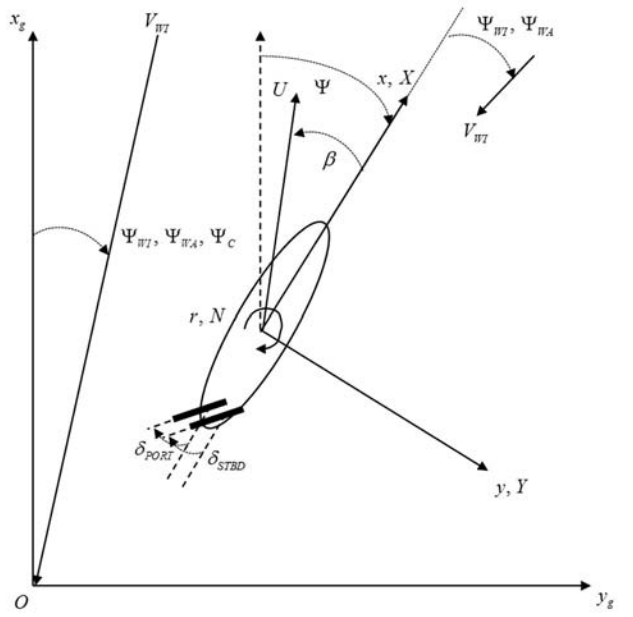

Fig. 1. Coordinate system.

Table 1
Definition of sea conditions (Bhattacharyya, 1978).

Beaufort number [−]	0	1	2	3	4	5	6	7	8
Maximum Wind speed [knots]	1	3	6	10	16	21	27	33	40
Significant wave height [m]	0	0.01	0.5	1.8	4.7	7.3	12.3	18.6	29.1

Twin propeller thrust loads are calculated as shown in Eq. (4). t indicates the thrust reduction coefficient, n is the propeller Revolutions Per Second (RPS), and K_T indicates the thrust coefficient. It is assumed that K_T depends only on the advance ratio marked as J_P. y_P is the distance from the center line to the installed propeller along the transverse axis and y_R is the distance from the center line to the installed rudder along the transverse axis. w_P is the wake fraction at the position of the propeller.

$$\begin{aligned} X_P &= (1-t)\cdot\rho\cdot {n_{PORT}}^2\cdot D_P^4 \bullet K_T(J_{P,\ PORT}) \\ &\quad +(1-t)\cdot\rho\cdot {n_{STBD}}^2\cdot D_P^4 \bullet K_T(J_{P,\ STBD}) \\ N_P &= y_P(1-t)\cdot\rho\cdot {n_{PORT}}^2\cdot D_P^4 \bullet K_T(J_{P,\ PORT}) \\ &\quad -y_P(1-t)\cdot\rho\cdot {n_{STBD}}^2\cdot D_P^4 \bullet K_T(J_{P,\ STBD}) \end{aligned} \quad (4)$$

where,

$J_{P,\ PORT} = u(1-w_P)/n_{PORT}D_P$

$J_{P,\ STBD} = u(1-w_P)/n_{STBD}D_P$

Twin rudder loads are calculated as shown in Eq. (5). F_{N_PORT} and F_{N_STBD} indicate the generated normal pressure on rudders installed on the port and starboard sides, respectively. t_R is the correction factor of the resistance increase due to steering, a_H is the fraction of increase of sway force due to steering, x_R is the rudder location, x_H is the point of application of additional sway force due to steering, y_R is the distance from the center line to the installed rudder along the transverse axis, and A_R is the area of each rudder. U_{R_PORT} and U_{R_STBD} indicate the velocity of the flow at the rudder locations on the port and starboard sides, respectively. $C_{L,\ \alpha}$ is the slope of the lift coefficient calculated using the aspect ratio of each rudder (Fujii and Tsuda, 1961, 1962). Because full spade rudders are equipped, the empirical formulas are used. The mathematical model is constructed as described.

$$\begin{aligned} X_R &= -(1-t_R)F_{N\_PORT}\cdot\sin\delta_{PORT} - (1-t_R)F_{N\_STBD}\cdot\sin\delta_{STBD} \\ Y_R &= -(1+a_H)F_{N\_PORT}\cdot\cos\delta_{PORT} - (1+a_H)F_{N\_STBD}\cdot\cos\delta_{STBD} \\ N_R &= -(x_R+a_Hx_H)F_{N\_PORT}\cos\delta_{PORT} - (x_R+a_Hx_H)F_{N\_STBD}\cos\delta_{STBD} \\ &\quad +y_R(1-t_R)F_{N\_PORT}\cdot\sin\delta_{PORT} + y_R(1-t_R)F_{N\_STBD}\cdot\sin\delta_{STBD} \end{aligned}$$

where,

$$\begin{aligned} F_{N\_PORT} &= 0.5\cdot\rho\cdot A_R^2\cdot {U_{R\_PORT}}^2\cdot C_{L,\alpha}\cdot\sin\alpha_{R\_PORT} \\ F_{N\_STBD} &= 0.5\cdot\rho\cdot A_R^2\cdot {U_{R\_STBD}}^2\cdot C_{L,\alpha}\cdot\sin\alpha_{R\_STBD} \\ C_{L,\alpha} &= \frac{6.13\Lambda}{\Lambda+2.25} \\ \alpha_{R\_PORT} &= \delta_{PORT} - \gamma\left(\beta - l'_R r'\right) \\ \alpha_{R\_STBD} &= \delta_{STBD} - \gamma\left(\beta - l'_R r'\right) \end{aligned} \quad (5)$$

As mentioned above, a comparison was made between the simulated results for the 35° turning test, the 10°/10° zigzag test, and the 20°/20° zigzag test at the design speed and those obtained from free running model tests. It is confirmed that simulated results are well matched with those obtained from the free running model tests (You et al., 2017).

2.2.2. Hydrodynamic loads due to wind

Wind loads can be calculated as shown in Eq. (6). Wind load coefficients which are denoted as C'_X, C'_Y, and $C'_N$are obtained from the empirical formulas (Fujiwara et al., 2001). The input values used to predict the coefficients have been summarized in previous research (You et al., 2017). A_T and A_L indicate the transverse and lateral projected area, respectively. ρ_{air} indicates the density of air and L_{OA} is the overall length of the ship. Irregular wind speeds which are relatively obtained denoted as V_{rWI} are considered as disturbance acting on the ship.

$$\begin{aligned} X_{WI} &= C'_X\cdot\frac{1}{2}\cdot\rho_{air}\cdot A_L\cdot {V_{rWI}}^2 \\ Y_{WI} &= C'_Y\cdot\frac{1}{2}\cdot\rho_{air}\cdot A_T\cdot {V_{rWI}}^2 \\ N_{WI} &= C'_N\cdot\frac{1}{2}\cdot\rho_{air}\cdot A_L\cdot L_{OA}\cdot {V_{rWI}}^2 \end{aligned} \quad (6)$$

Eq. (7) shows the definition of relative wind speed along the x-axis, y-axis. And relative wind speed denoted as V_{rWI} and relative wind incident angle denoted as ψ_{rWI} are defined. The Froya spectrum is used to obtain the spectral density function considering representative wind speed, and irregular wind speeds are then generated (You et al., 2017; Andersen and Løvseth, 1992).

$$
\begin{aligned}
u_{rWI} &= V_{WI}\cos(\psi_{WI}-\psi)+u\\
v_{rWI} &= V_{WI}\sin(\psi_{WI}-\psi)+v\\
V_{rWI} &= \sqrt{(u_{rWI})^2+(v_{rWI})^2}\\
\psi_{rWI} &= \tan^{-1}(v_{rWI}/u_{rWI})
\end{aligned}
\tag{7}
$$

2.2.3. Hydrodynamic loads due to waves

To consider the wave loads acting on the container ship, the ship design information were used. The concept of a linear superposition is used to calculate the wave drift forces and the moment in irregular waves. The increase in mean resistance in irregular waves is calculated by using pre-calculated wave drift forces and moment and wave spectrum. It is written as follows, and the process is well summarized in reference (International Organization for Standardization (ISO) 15016, 2015; International towing tank Conference (ITTC), 2011).

$$
X_{WA}, Y_{WA}, N_{WA} = \int_0^\infty \frac{QTF(w,\alpha)}{\zeta_A^2} E(w)dw
$$

$$
E(w) = \frac{5}{16}H_S^2\frac{w_m^4}{w^5}\exp\left\{-\frac{5}{4}\left(\frac{w_m}{w}\right)^4\right\}
$$

$$
\begin{aligned}
&where,\\
&w : mean\ wave\ frequency\\
&\alpha : angle\\
&\zeta_A : amplitude\\
&E(w) : ITTC\ wave\ spectrum\\
&H_S : significant\ wave\ height\\
&w_m : modal\ wave\ freqency
\end{aligned}
\tag{8}
$$

The wave drift forces and moment for the surge, sway, and yaw is calculated for the design condition. HYDROSTAR, provided by Bureau Veritas (BV) classification, is used here. The wave drift forces and moment for X, Y, and N at an arbitrary time are obtained by using the linear interpolation method according to the relative wave incident angle.

Fig. 2 shows the non-dimensionalized surge, sway, and yaw wave drift forces and moment for 60° waves of the container ship with design draft and design speed. The black solid line, blue chain line, and red broken line indicate results for the surge, sway, and yaw wave drift forces and moment, respectively. The typical tendencies of the wave drift force are well shown in these figures.

2.2.4. Hydrodynamic loads due to current

Definition of relative speed for current can be calculated as shown in Eq. (9). u_{rC} and v_{rC} indicate the relative speed of the ship with the current along the x-axis and y-axis. The relative speeds are used to calculate hydrodynamic loads acting on the hull considering current (Hwang, 1980).

$$
\begin{aligned}
u_{rC} &= V_C\cos(\psi_C-\psi)+u\\
v_{rC} &= V_C\sin(\psi_C-\psi)+v
\end{aligned}
\tag{9}
$$

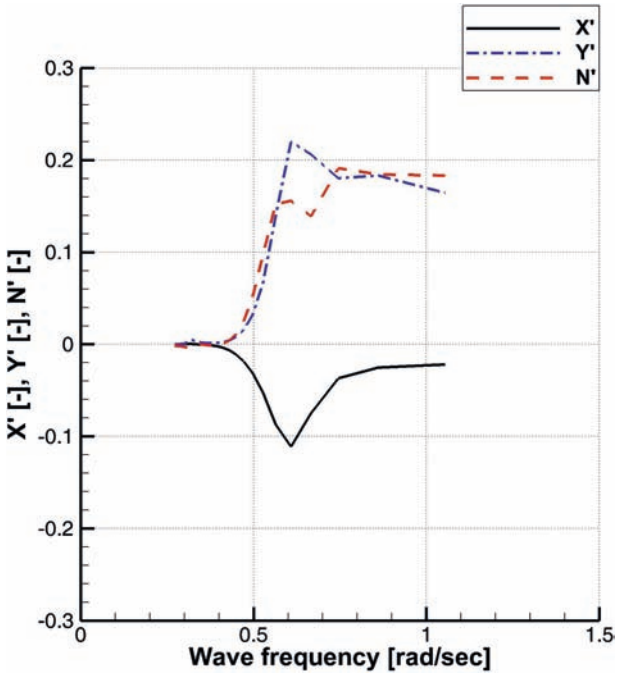

Fig. 2. Nondimensionalized surge, sway and yaw wave drift forces and moment for 60° waves.

3. Simulation concept to quantify sailing safety of a ship

In offshore structures constructed for drilling and production, a Dynamic Positioning (DP) system can be used to maintain the specified location of a vessel under various environmental conditions. The performance of a DP vessel needs to be quantified, and the DP capability chart is representatively used to indicate the capability of the DP vessel (Hendzik, 2013). Like DP capability chart, polar capability charts are used to indicate the performance of a ship, as well (Prpic-Orsic et al., 2016; Papanikolaou and Shigunov, 2014). Based on the polar chart, an operating instruction can be given or the thruster capacity can be determined. We focused on the similarity between the purposes of a DP system and an autopilot system. The purpose of an autopilot system is to follow a planned route within an allowable error. From the similarity of the two systems, sailing safety was quantified (You et al., 2017). Here, the quantified concept is developed as a safe operation capability chart of a ship for use as the basis of design.

Fig. 3 shows the flow chart to obtain a safe operation capability chart. To assess the safe operation capability, it is the most important to judge whether the ship can be safely operated or not. In Fig. 3, some steps are added to develop a safe operation capability chart from the safe operation judgment chart and colored boxes indicate the added steps in this work. Fig. 4 shows the basic concept used to quantify sailing safety in oceans (You et al., 2017). The same concept is applied in this study.

First of all, it is assumed that a ship follows virtual way points that are located along a straight line as shown in Fig. 4

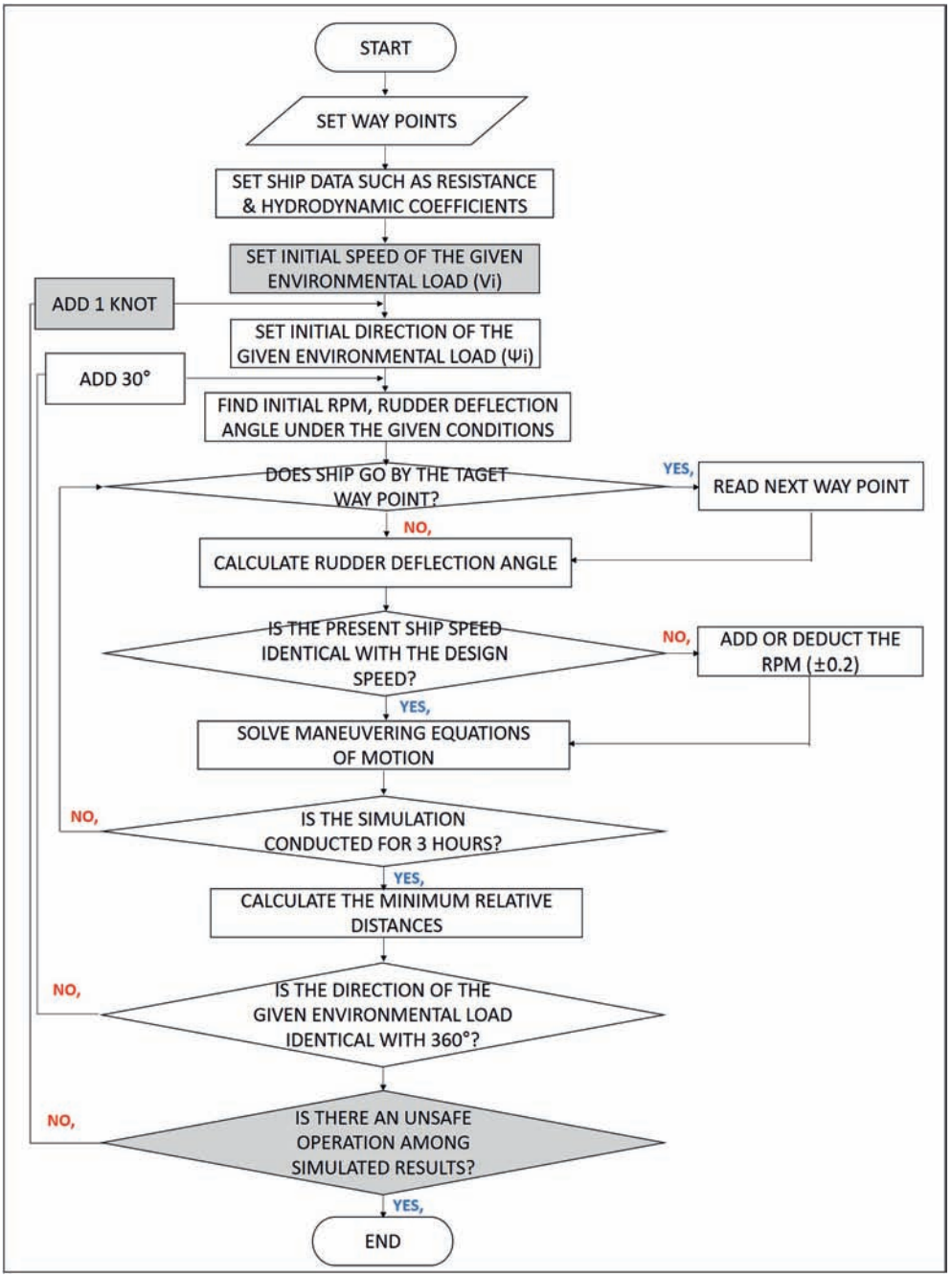

Fig. 3. Flow chart to obtain a safe operation capability chart.

if we start a simulation to assess the safe operation capability. The way points are generated at the intervals of distance by which a ship can move for 1 min at its present speed (You and Rhee, 2016).

And, ship data including principal particulars, resistance coefficient, and hydrodynamic coefficients are set. Here, a twin-screw container ship is studied and the design information and model test data etc. are inputted.

And we have to determine that which environmental load is considered to assess the safe operation capability. Of course, plural environmental loads can be considered at the same time. Even if an environmental load among the considered loads can be regarded as fixed one, collinear one, and non-collinear one. For easier understanding in the flow chart, the basic concept is only explained for the wind. If plural loads have to be considered at the same time, the values related to environmental loads have to be changed according to the intended condition.

The initial speed of an environmental load has to set. 1.0 knot is assumed to the smallest speed to evaluate the safe operation capability, here. And the initial direction of the environmental load has to set as 0°. Before maneuvering simulation is conducted by following the way points, initial conditions such as Revolution Per Minute (RPM), rudder

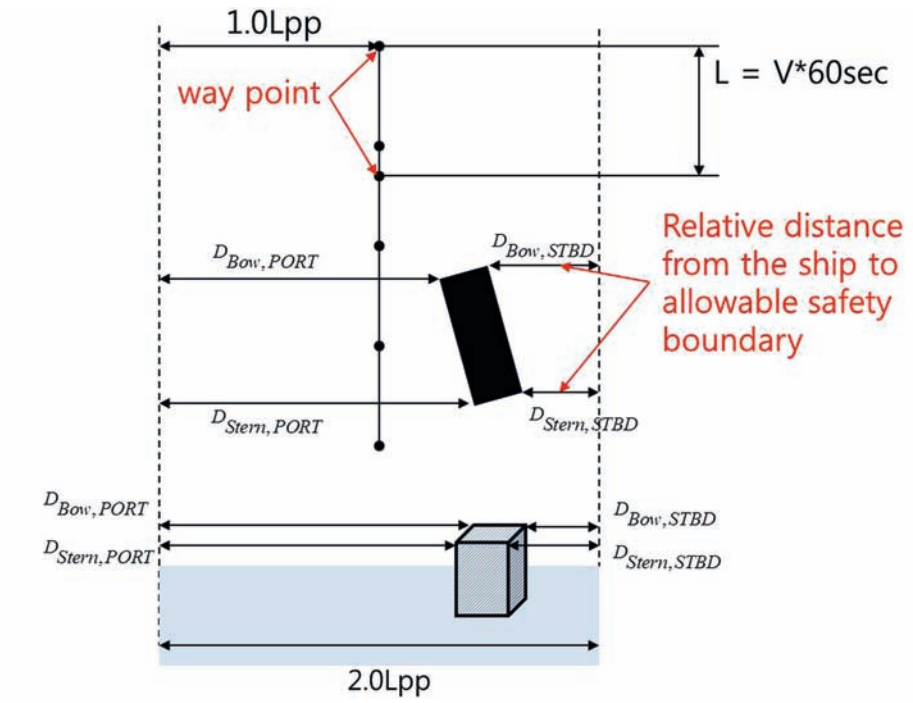

Fig. 4. Concept used to quantify sailing safety in oceans.

deflection angle to maintain ship's speed and course under the given environmental condition have to be found.

A simulation starts using the prescribed information by following the assumed way points. If the ship goes over the target way point, then next way point is substituted as the existing way point. Otherwise, the existing way point will be maintained. If attempts are made to maintain a ship at a certain course under various environmental, it is essential that the rudder deflection angle is also changed. Here, the rudder deflection angle is controlled by using the fuzzy control at every time step during the simulations. Two inputs are combined to determine rudder angle. They are the difference from ship's heading angle to the virtual way point and turn rate of the ship.

If attempts are made to maintain a ship at a certain speed under various environmental conditions (in which additional resistances due to the wind and current are successively changed), it is necessary that the RPM is also changed. By comparing the target speed and the present speed, RPM is added or deducted by 0.2 every 60 s. Maneuvering equations of motion are solved every 0.5 s using the obtained information.

Automatic navigation is conducted under a certain error between a planned route and an actual location. Obviously, the allowable error depends on an equipped system. In the previous study, 0.2 N mile is used to judge the safe operation by referring to the allowable safe boundaries used for an autopilot system (You et al., 2017). Common criteria are necessary to develop an approach to determine rudder area in spite of different type of a ship and different size of a ship. 1.0 Lpp is regarded as a critical distance for an evaluated collision risk in a collision avoidance algorithm, the allowable safe boundaries are assumed as 1.0 Lpp, here.

A ship is assumed as a rectangle of which the length is *Lpp* and breadth is *B*. After calculating the relative distances, which are denoted as $D_{Bow,\ STBD}$, $D_{Stern,\ STBD}$, $D_{Bow,\ PORT}$, and $D_{Stern,\ PORT}$ between four edges of the assumed rectangle and allowable safe boundaries along the transverse axis for 3 h, the minimum value is acquired.

Transient maneuvering behaviors occur due to wind and current at the beginning of each simulation. It is necessary to exclude the obtained minimum distance during the transient period because stable maneuvering behaviors are only considered for evaluating the maneuvering capability of the ship. However, the transient periods differ according to the sailing speed and magnitude of environmental loads. Here, simulations for the initial 2 h are excluded, after which simulations are conducted for 5 h. The reason why the duration is assumed as 3 h is that a full 3 h simulation period for each load case is recommended in the analyses, if applicable in time domain analyses (DET NORSKE VERITAS (DNV), 2011).

If the calculations are not conducted in the range from 0° to 360° at intervals of 30°, 30° is added at an incident angle and identical calculation is repeated. If the calculations are done for all range, it is searched whether an unsafe operation is observed at least one incident angle. If the minimum value is smaller than 0 m, then the ship has invaded the allowable safe boundaries and this is judged as an unsafe operation. If there is no unsafe operation, prescribed simulations are repeatedly conducted under increased wind speed from 1 knots to 40 knots at intervals of 1 knot. And, at least one unsafe operation is observed, present wind speed is regarded as unsafe condition and the maximum

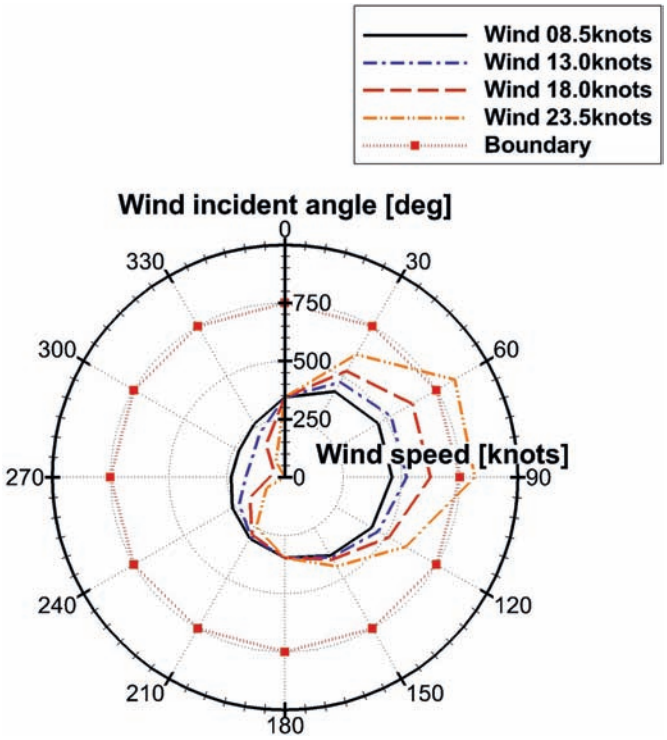

Fig. 5. Example of a safe operation judgment chart of a ship with service speed under various winds (You et al., 2017).

allowable speeds are marked on a polar plot. The envelope in this study is called a safe operation capability chart.

Fig. 5 shows an example of a safe operation judgment chart of a container ship with service speed under various wind conditions. This chart is only plotted for $D_{Bow,\ STBD}$. The radius from this chart indicates the magnitude of the minimum relative distances. The black solid line, blue chain line, red broken line, and orange two-point chain line, and red dotted line with squares indicate the results under 8.5 knots wind, 13.0 knots wind, 18.0 knots wind, and 23.5 knots wind, respectively. The red solid line indicates 750.0 m and is two times the Lpp along the transverse axis.

If a calculated relative distance is smaller than 0 m, it indicates that the edge of the bow and starboard side is outside the allowable safe boundaries to the starboard side. Likewise, if a calculated relative distance is larger than the red solid line, then the edge of the bow and starboard side is outside the allowable safe boundaries in the opposite direction. If winds are from the starboard side, $D_{Bow,\ STBD}$ are increased because the ship is biased to the port side. In contrast, $D_{Bow,\ STBD}$ are decreased due to winds from the port side. Ideally, if four edges maintain 345.5 m, the ship follows the virtual way points without disturbance.

As wind speed decrease, the disturbed effect of the ship becomes small. It is known that the ship under 23.5 knots winds is more disturbed than that under 8.5 knots winds. And winds from 60° to 300° are most critical because the magnitude of the minimum relative distances with 60° wind is the largest and the magnitude of the minimum relative distances with 300° wind is the smallest.

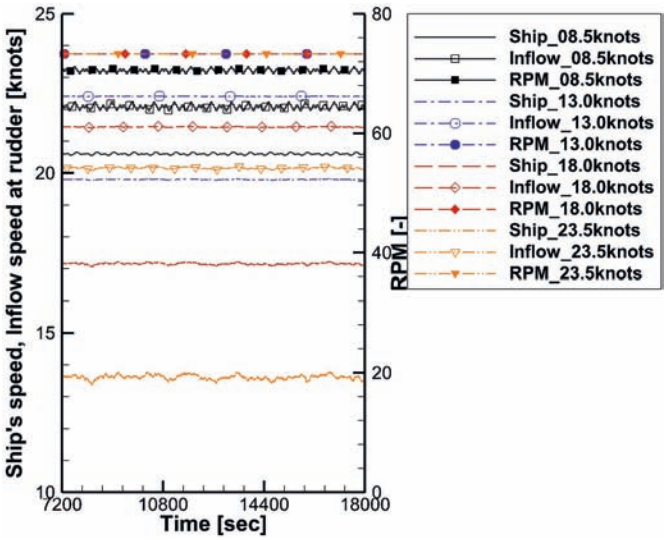

Fig. 6. Time histories of ship's speed, inflows speed at rudder, and RPM of a ship with service speed under various winds.

Fig. 6 shows the time histories of ship's speed, inflows speed at the rudder, and RPM of a ship with service speed under various wind conditions. The simulated wind speeds are identical with those in Fig. 5. The wind incident angle is fixed as 60°. The definition of each line is summarized in the figure. The marked data are from 7200 s to 18,000 s to exclude initial transient period.

The ship's speed according to wind speed is different. If the wind speed increase, the additional resistance acts on the hull and it makes the ship slow. To maintain ship's speed as design speed, RPM is increased from initial RPM to the maximum RPM. In the case of 8.5 knots wind, the ship's speed can be maintained at the design speed. However, the added resistance due to 13.0 knots, 18.0 knots, and 23.5 knots wind cannot be balanced with present propulsion specification. The RPMs for 13.0 knots, 18.0 knots, and 23.5 knots wind have the maximum values in the figure.

Inflow speed at rudder is affected by ship speed and RPM of the propeller. The maximum inflow speed is observed with 13.0 knots wind. Because the RPM for 13.0 knots wind is larger than that for 8.5 knots wind, the inflow speed for 13.0 winds is larger than that for 8.5 knots wind, even if the ship's speed for 13.0 knots wind is smaller than that for 8.5 knots wind. Because RPMs for 13.0 knots, 18.0 knots, and 23.5 knots wind are identical as the maximum value, the inflows speed is affected by ship's speed. Consequently, the inflow speed decrease according to the ship's speed.

Fig. 7 shows an example of a safe operation capability chart of a container ship with service speed under winds, only. The envelope is similar to those of the DP capability chart (Hendzik, 2013). The envelope is almost symmetric to the port side and starboard side.

When winds are from 0° or 180°, no disturbance occurs to the transverse direction. Therefore, the ship can follow way points without disturbance in any case. Therefore, the maximum wind speed is 40 knots. The minimum capability is

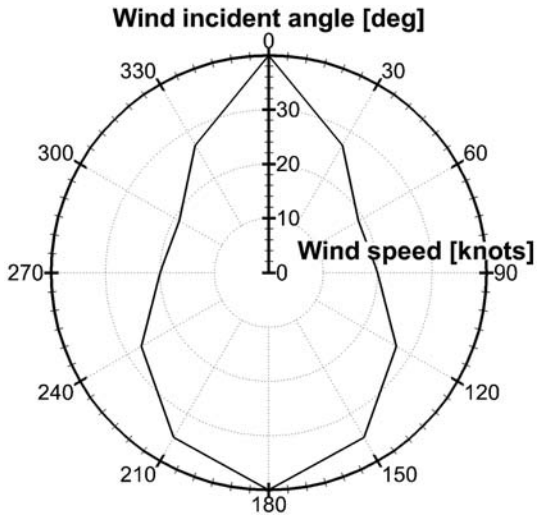

Fig. 7. Example of a safe operation capability chart of a ship with service speed under winds.

observed when winds are from 60° or 300°. In the DP capability charts, the critical wind direction is frequently from 30° to 60° due to the tendency of wind load coefficients. Likewise, the safe operation capability chart is affected by wind load characteristics of the container ship.

Fig. 8 shows an example of a safe operation judgment chart of a container ship with service speed under various current conditions. This chart is only plotted for $D_{Bow,\ STBD}$, as well. The radius from this chart indicates the magnitude of the minimum relative distances. The black solid line, blue chain line, red broken line, and orange two-point chain line, and red dotted line with squares indicate the results under 0.25 knots current, 0.50 knots current, 0.75 knots current, and 1.00 knots current, respectively. The meanings of red dotted line with squares and magnitude of relative distance are identical with prescribed description. If currents are from the starboard side, $D_{Bow,\ STBD}$ are increased because the ship is biased to the port side. In contrast, $D_{Bow,\ STBD}$ are decreased due to currents from the port side. Ideally, if four edges maintain 345.5 m, the ship follows the virtual way points without disturbance. As current speed decrease, the disturbed effect of the ship becomes small. It is known that the ship under 1.00 knots current is more disturbed than that under 0.25 knots winds. And current from 90° to 270° are most critical because the magnitude of the minimum relative distances with 90° current is the largest and the magnitude of the minimum relative distances with 270° wind is the smallest.

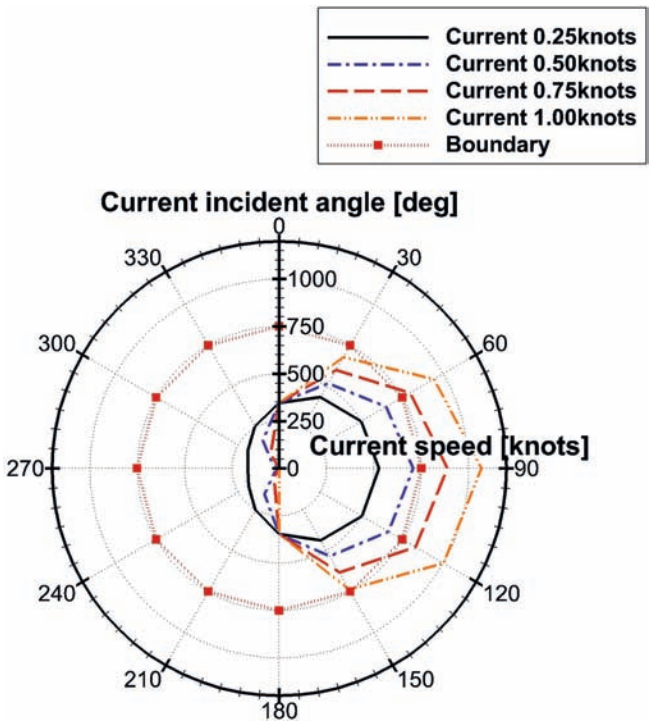

Fig. 8. Example of a safe operation judgment chart of a ship with service speed under various currents (You et al., 2017).

Fig. 9 shows the time histories of ship's speed, inflows speed at the rudder, and RPM of a ship with service speed under various current conditions. The simulated current speeds are identical with those in Fig. 8. The current incident angle is fixed as 30°. The definition of each line is summarized in the figure. The ship's speed according to current speed is almost same. To maintain ship's speed as design speed, RPM is increased as shown in the figure. Inflow speed at rudder is affected by RPM of the propeller. The maximum inflow speed is observed with 1.00 knots current.

Fig. 10 shows an example of a safe operation capability chart of a container ship with service speed under currents. The envelope is almost symmetric to the port side and starboard side. When currents are from 0° or 180°, no disturbance occurs in the transverse direction. Therefore, the ship can follow way points without disturbance in any case. Therefore, the maximum current speed is 1 knot. The minimum capability is observed when currents are from 90° or 270°.

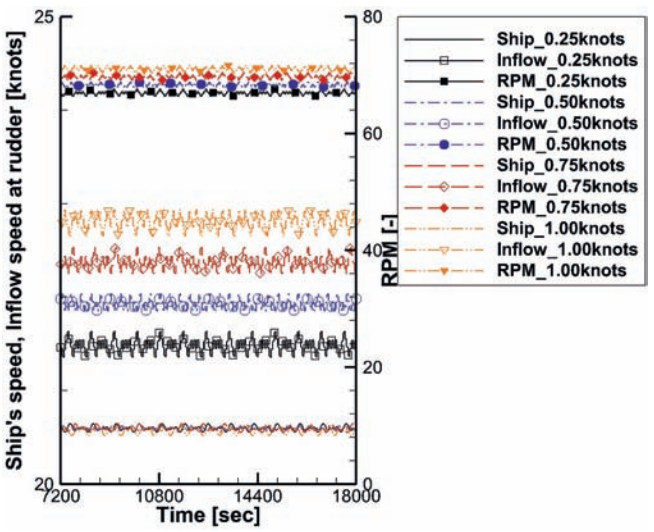

Fig. 9. Time histories of ship's speed, inflows speed at rudder, and RPM of a ship with service speed under various currents.

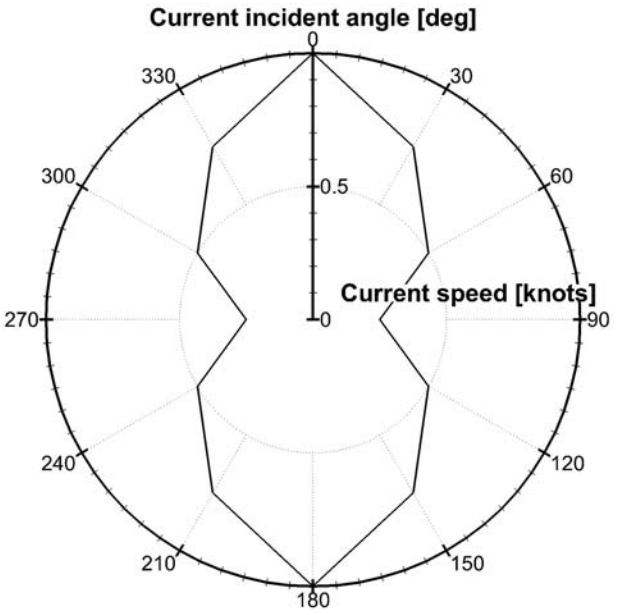

Fig. 10. Example of a safe operation capability chart of a ship with service speed under currents.

4. Calculations and discussion of a safe operation capability chart as design basis

Sailing safety is only quantified under wind and current in the previous research (You et al., 2017). If a new approach to determine a design basis of a rudder is developed based on a safe operation capability chart, the effect of waves has to be additionally considered since the operation performance of a ship is synthetically affected by the wind, wave and current (International Organization for Standardization (ISO) 15016, 2015; Prpic-Orsic et al., 2016; Papanikolaou and Shigunov, 2014; Sutulo and Soares, 2015, 2016). To construct a capability chart as a design basis, two assumptions are additionally used. First, the wave is collinear with wind. Second, the significant wave height is always proportional to the wind speed.

In the Ref, sea conditions are defined (Bhattacharyya, 1978). The range of wind speed and wave information is summarized (Bhattacharyya, 1978). Here, the maximum wind speed is assumed to be proportional to significant wave height as shown in Table 1. To generate wave spectrum, the wave period is additionally needed. Eq. (10) shows the range of probable peak wave periods (GL Noble Denton, 2010). In this research, the representative value is assumed as $T_P = \frac{\sqrt{13 \cdot H_{1/3}} + \sqrt{30 \cdot H_{1/3}}}{2}$. Consequently, wave loads are calculated using significant wave height, peak period, and wave direction which are obtained from assumed wind speed and direction.

$$\sqrt{13 \cdot H_{1/3}} < T_P < \sqrt{30 \cdot H_{1/3}} \tag{10}$$

As explained, a safe operation capability chart can be obtained from repeated simulations with different wind speeds ranging from 0 knots to 40 knots at intervals of 1 knot. Since wave condition is decided according to the wind condition, any sign is not marked on the capability chart. Just, the effect of the wave is considered on the plotted capability. In the case of current, the safe operation capability is sensitively assessed according to the current incident direction. The safe operation capability chart is only investigated for current from the head sea and the following sea.

Before the safe operation capability charts are confirmed for use as the basis of design, it is necessary to investigate the appropriateness of the capability chart as a new design approach by comparing it with a conventional approach based in IMO maneuvering tests. For this purpose, different rudders are assumed as shown in Table 2, which provides information on alternative rudders. Four different rudders are used, although each rudder has the same aspect ratio of 1.40.

Because the mathematical model of the container ship has already been verified with rudder 2, rudder 2 is regarded as the benchmark case. Rudder 1 is tested to consider the effect of the rudder, the area of which is 10% greater than that of the benchmark case. Rudder 4 is obtained from a rule proposed by GL and the rudder area is 12.5% smaller than the benchmark case (Germanischer Lloyd (GL), 2013).

The rule is shown in Eq. (11), where L is 375.0 m, T is 16.0 m, and c_1, c_2, c_3, c_4 are 1.0. The acquired minimum area is denoted as A_R, which is 105.0 m^2. As the twin-screw container ship is considered, each area of a rudder is assumed to be 52.5 m^2. Rudder 3 is tested to consider the effect of the rudder, and the area is 15% less than that of the benchmark case. In addition, the area of rudder 3 is determined as smaller than that obtained from the GL rule.

$$A_R = c_1 \cdot c_2 \cdot c_3 \cdot c_4 \frac{1.75 \cdot L \cdot T}{100}$$

$$\begin{aligned} &where, \\ &c_1 : factor\ for\ the\ ship\ type \\ &c_2 : factor\ for\ the\ rudder\ type \\ &c_3 : factor\ for\ the\ rudder\ profile \\ &c_4 : factor\ for\ the\ rudder\ arrangement \end{aligned} \tag{11}$$

Table 2
Information of alternative rudders.

	Rudder 1	Rudder 2	Rudder 3	Rudder 4
Aspect ratio [−]	1.40			
Area [m^2]	66.00	60.0	51.00	52.50
Relative ratio [%]	110.0	100.0	85.0	87.5

Table 3
Designed condition for maneuvering simulations.

Item	Data	
Design speed [*knots*]	20.6	
Designed allowable safe boundaries [*Lpp*]	1.0	
Current speed [*knots*]	2.0	
Current direction [*deg*]	0	180
Target wind speed [*knots*]	19.0	

Table 3 shows the designed condition for maneuvering simulations. The design speed is 20.6 knots, and the allowable safe boundaries are assumed to be 1.0 Lpp. In addition, three current conditions are used: no current, 2 knots from 0°, and 2 knots from 180°. And, we assumed a target wind speed as 19.0 *knots* which is representative wind speed under sea state 5 (Bhattacharyya, 1978). Here, the target wind speed is an example to review the appropriateness as the basis of design.

First, IMO maneuvering tests are simulated to check the effects of rudder area on maneuverability. From the comparison, the rudder area can be determined by following a conventional approach. Fig. 11 shows the trajectories for the initial turning tests of the container ship with four different rudders. The black solid line, blue chain line, red broken line with squares, and green two point chain line refer to the results for rudders 1, 2, 3, and 4, respectively.

The differences between plotted trajectories are insignificant. Table 4 shows relative ratios between the predicted initial track reaches of the container ship with rudders 1, 3, and 4 for initial turning tests and those with rudder 2. Even if rudder 1 is 10% larger than that of the benchmark rudder, the initial track reach is decreased by only 4%. Moreover, although rudder 3 is 15% smaller than the benchmark rudder, the initial track reach is increased by only 6%. Accordingly, the effect of rudder area on initial turning ability is not distinct.

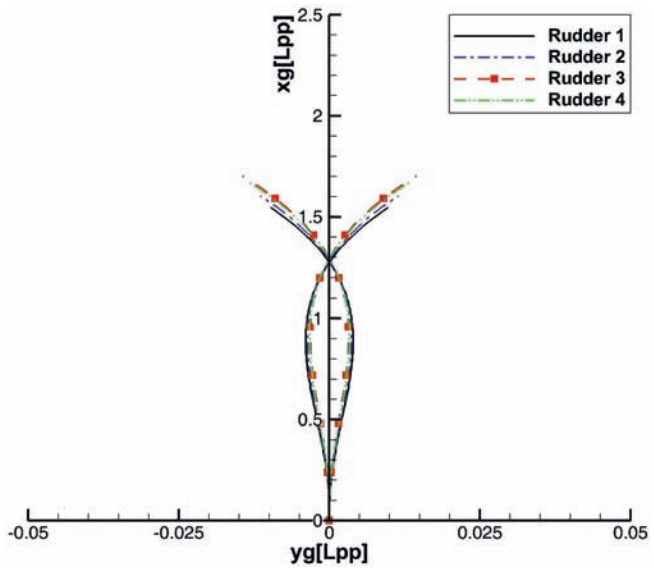

Fig. 11. Trajectories for initial turning tests of the container ship with four different rudders.

Table 4
Relative ratios between the predicted initial track reaches of the container ship with rudders 1, 3, and 4 for initial turning tests and those with rudder 2.

	Initial track reach
(Rudder 1/Rudder 2) * 100 [%]	96
(Rudder 3/Rudder 2) * 100 [%]	106
(Rudder 4/Rudder 2) * 100 [%]	105

Table 5
Relative ratios between the predicted advances, transfer, and tactical diameters of the container ship with rudders 1, 3, and 4 for 35° turning tests and those with rudder 2.

	Advance	Transfer	Tactical Diameter
(Rudder 1/Rudder 2) * 100 [%]	98	96	97
(Rudder 3/Rudder 2) * 100 [%]	104	106	104
(Rudder 4/Rudder 2) * 100 [%]	103	105	103

Fig. 12 shows the trajectories for 35° turning tests of the container ship with four different rudders. The definitions of each line are identical to those shown in Fig. 11. The differences between the plotted trajectories during the 35° turning tests are also insignificant. Table 5 shows the relative ratios between the predicted advances, transfer, and tactical diameters of the container ship with rudders 1, 3, and 4 for 35° turning tests and those with rudder 2. In the case of advances, transfers, and tactical diameters obtained from 35° turning tests, the variation according to rudder area is less than that of the initial turning tests. In the case of rudder 1, the values deviated only by 2%, 4%, and 3%. For the smallest rudder, rudder 3, the values are deviated only by 4%, 6%, and 4% for advances, transfers, and tactical diameters, respectively. Determining a rudder area based on the turning tests creates ambiguity, because all values meet the IMO maneuvering criteria related to turning characteristics and the difference between values with different rudders is insignificant.

Figs. 13 and 14 show the time histories of the heading angle of the container ship for the 10°/10° zigzag test and 20°/20° zigzag test, respectively, to port side with four different rudders. The definitions of each line are the same as those in Fig. 11. As the rudder area increases, the 1st and 2nd overshoot angles increase and the times at peaks are delayed. Table 6 shows the relative ratios between the predicted 1st and 2nd

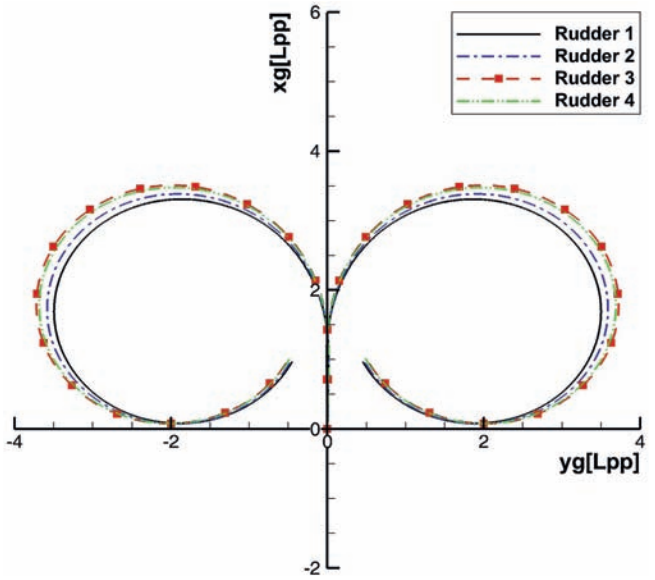

Fig. 12. Trajectories for 35° turning tests of the container ship with four different rudders.

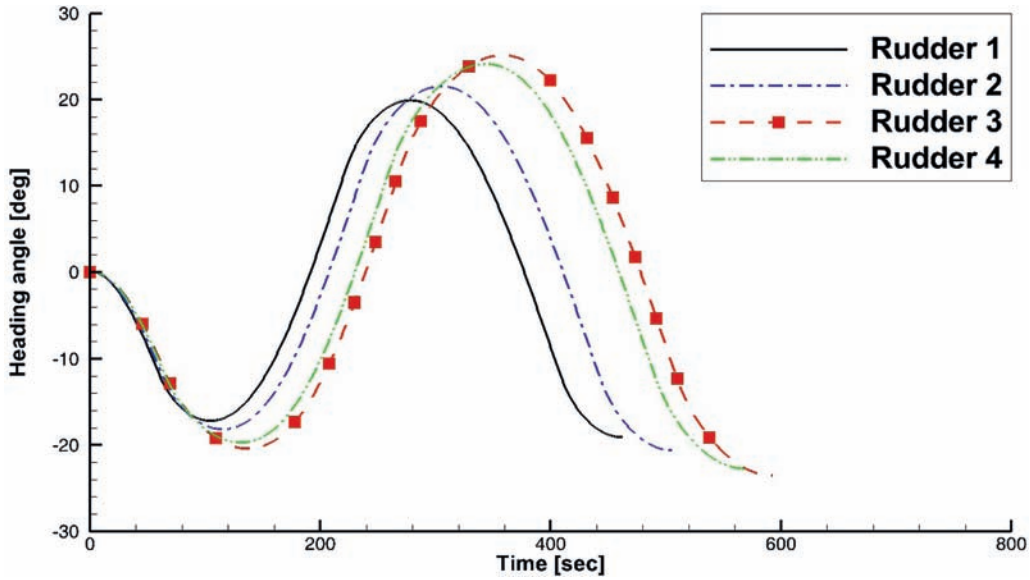

Fig. 13. Time histories of heading angle of the container ship for 10°/10° zigzag test to port side with four different rudders.

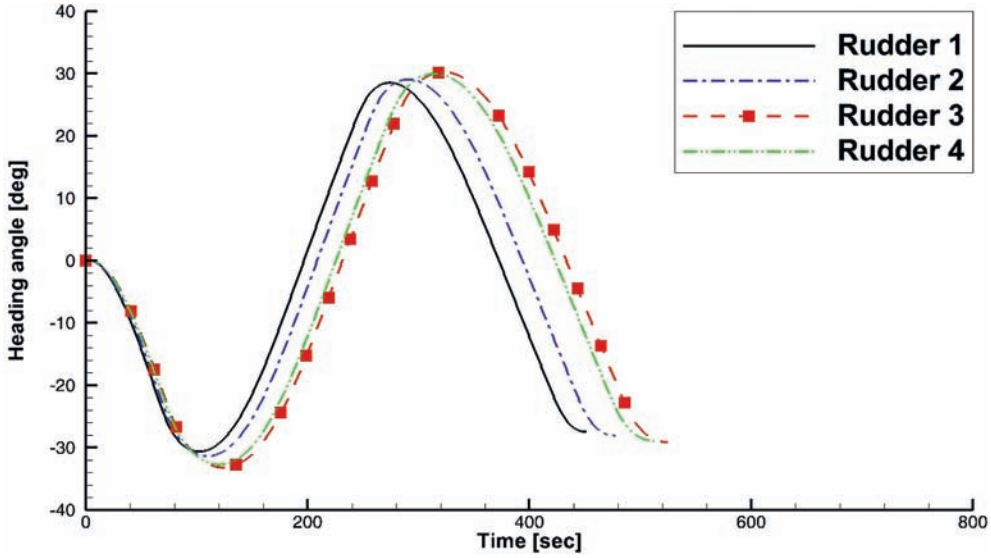

Fig. 14. Time histories of heading angle of the container ship for 20°/20° zigzag test to port side with four different rudders.

Table 6
Relative ratios between the predicted 1st and 2nd overshoot angles of the container ship with rudders 1, 3, and 4 for 10°/10° zigzag tests and those with rudder 2.

	1st overshoot angle	2nd overshoot angle
(Rudder 1/Rudder 2) * 100 [%]	88	86
(Rudder 3/Rudder 2) * 100 [%]	127	131
(Rudder 4/Rudder 2) * 100 [%]	119	123

Table 7
Relative ratios between the predicted 1st and 2nd overshoot angles of the container ship with rudders 1, 3, and 4 for 20°/20° zigzag tests and those with rudder 2.

	1st overshoot angle
(Rudder 1/Rudder 2) * 100 [%]	94
(Rudder 3/Rudder 2) * 100 [%]	116
(Rudder 4/Rudder 2) * 100 [%]	112

overshoot angles of the container ship with rudders 1, 3, and 4 for the 10°/10° zigzag tests and those with rudder 2. Table 7 show the relative ratios between the predicted 1st and 2nd overshoot angles of the container ship with rudders 1, 3, and 4 for the 20°/20° zigzag tests and those with rudder 2. If a rudder area is smaller than that of the benchmark rudder, considerable difference can be observed. But still, determining a rudder area based on the zigzag tests creates ambiguity. Since the overshoot angles for the container ship are extremely small, all values meet the IMO maneuvering criteria related to the 10°/

10° zigzag and 20°/20° zigzag tests. As described, it is difficult to judge the appropriateness of the designed rudder by comparing the results from the zigzag tests.

As described from Figs. 11–14, no clear design goals of the rudder can be found in the conventional approach. Because there are a lot of candidate design for a vessel by following the conventional design procedure, it is inevitable to determine rudder design on experience. Of course, this ambiguous application results from the superior maneuverability of the twin-screw container ship. However, the design approach needs to be applied to determine the rudder area in any case. Therefore, a new method of evaluating rudder performance for design needs to be found.

Especially, two essential factors are anticipated. First, rudder has to be designed from the quantified values. Second, the new approach can avoid the prescribed ambiguity among candidate design. Viewed in this way, the design approach by using safe operation capability charts are reviewed as follows.

Figs. 15–18 show the safe operation capability charts for the container ship with rudders 1, 2, 3, and 4 under different wind and current conditions, respectively. To investigate the effect of waves on the capability, wave loads are not considered. The black solid line, blue chain line, and red broken line indicate the results under no current, 2 knots from 0°, and 2 knots from 180°, respectively. As the assessed capability is sensitively affected according to the current incident direction, the conditions are restricted as no current, 0°, and 180°. From the results, the maximum wind speed for safe operation for every incident angle is observed from the results under 2 knots current from 0°. This indicates that the current from the head sea enables the course of the ship to be easily maintained. Rudder 1 can meet the target wind speed assumed in Table 2. Of course, all maneuvering test results for Rudder 1 can meet the criteria regulated by the IMO.

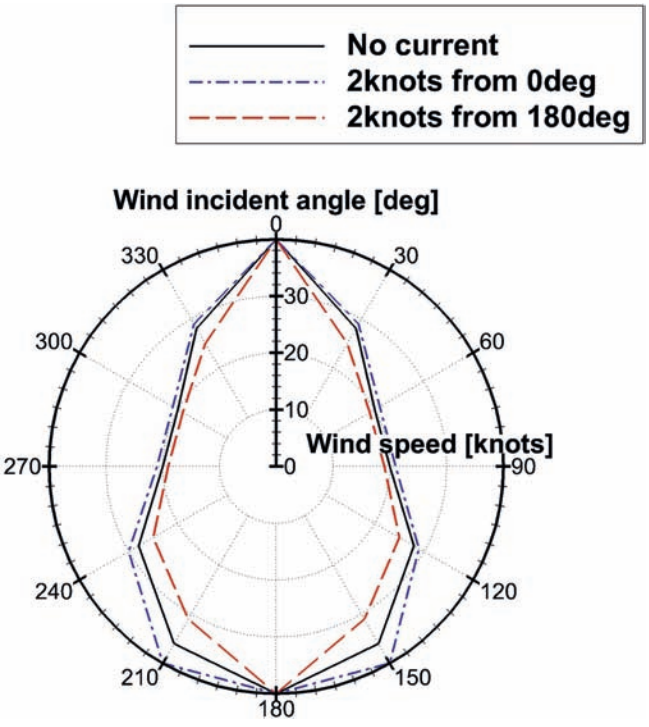

Fig. 15. Safe operation capability charts for the container ship with rudder 1 under wind and current.

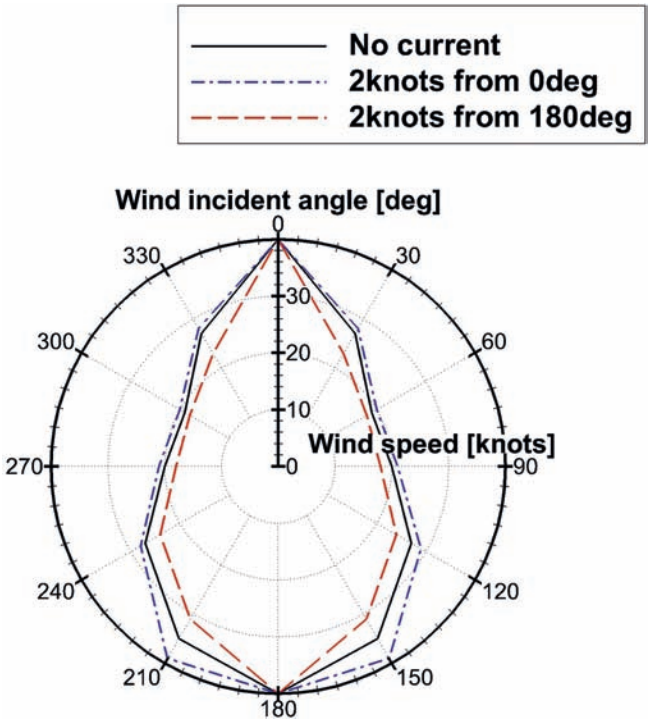

Fig. 16. Safe operation capability charts for the container ship with rudder 2 under wind and current.

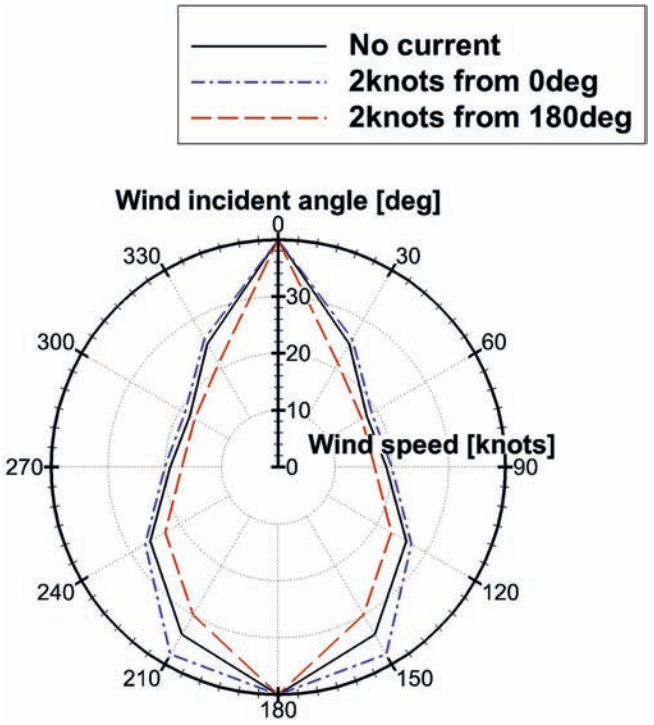

Fig. 17. Safe operation capability charts for the container ship with rudder 3 under wind and current.

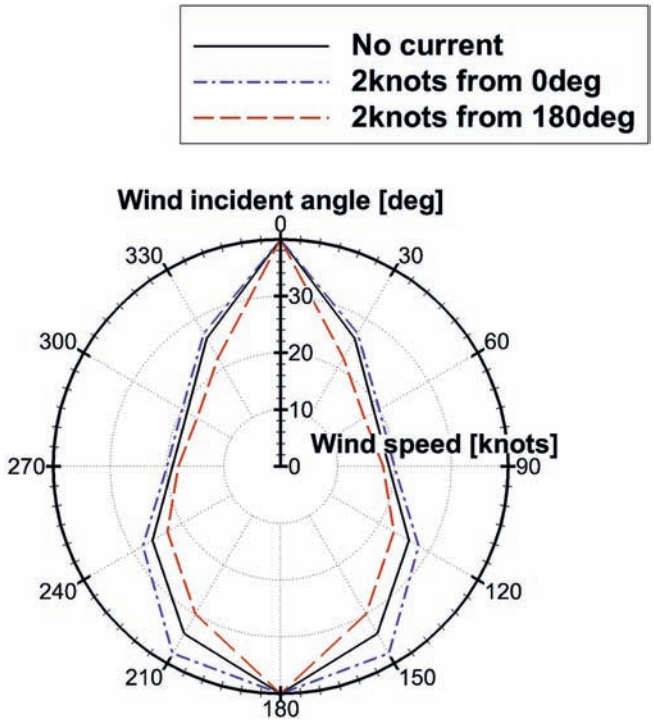

Fig. 18. Safe operation capability charts for the container ship with rudder 4 under wind and current.

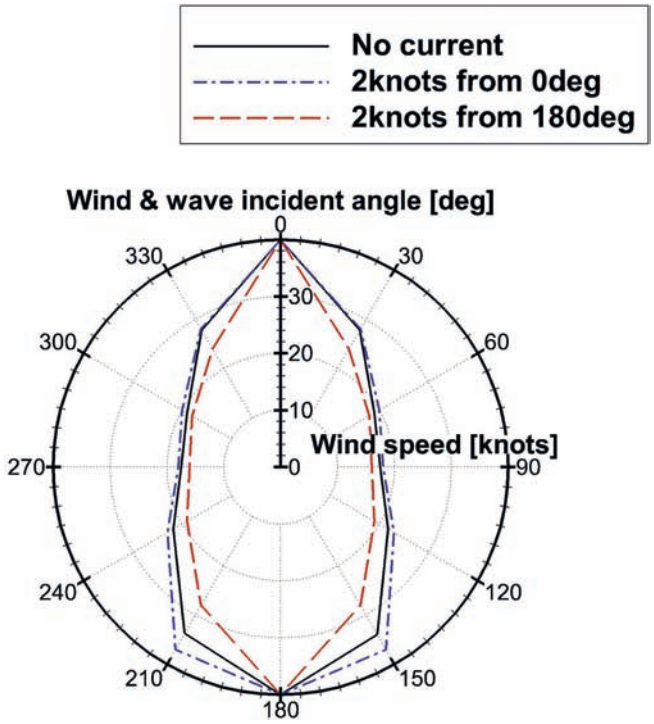

Fig. 19. Safe operation capability charts for the container ship with rudder 1 under wind, wave, and current.

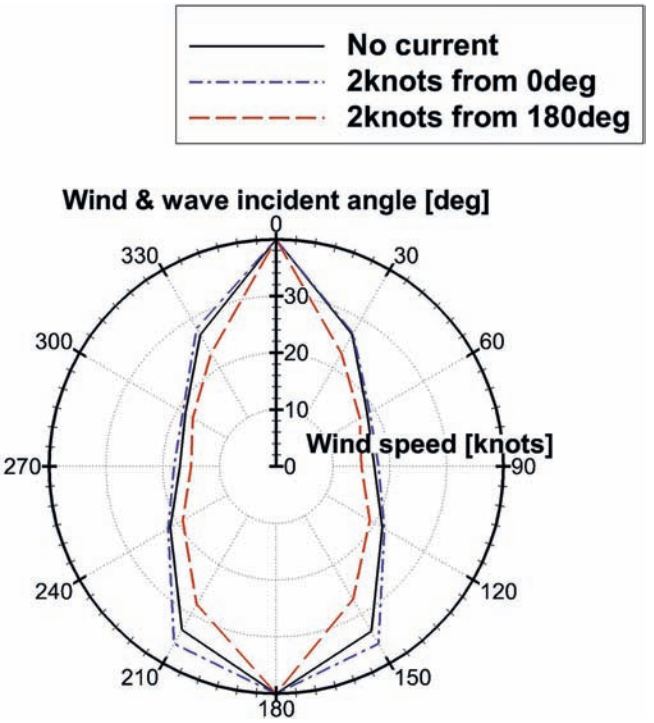

Fig. 20. Safe operation capability charts for the container ship with rudder 2 under wind, wave, and current.

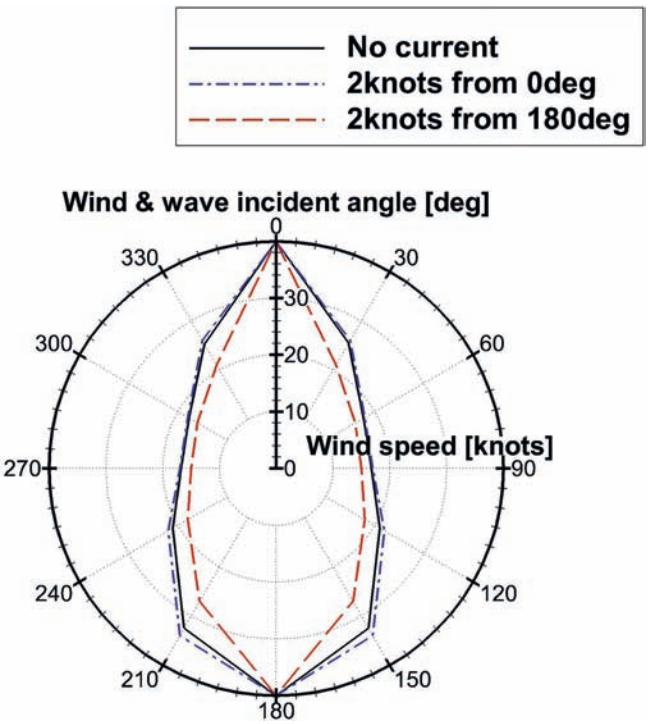

Fig. 21. Safe operation capability charts for the container ship with rudder 3 under wind, wave, and current.

Figs. 19–22 show the safe operation capability charts for the container ship with rudders 1, 2, 3, and 4 under different environmental conditions for wind, wave and current, respectively. By comparing the figures from 15 to 18, wave loads are additionally considered, here. The definitions of lines are identical with those used in Figs. 15–18. When wave loads are additionally considered, the shape of the capability chart is significantly affected. Especially, the maximum wind speeds

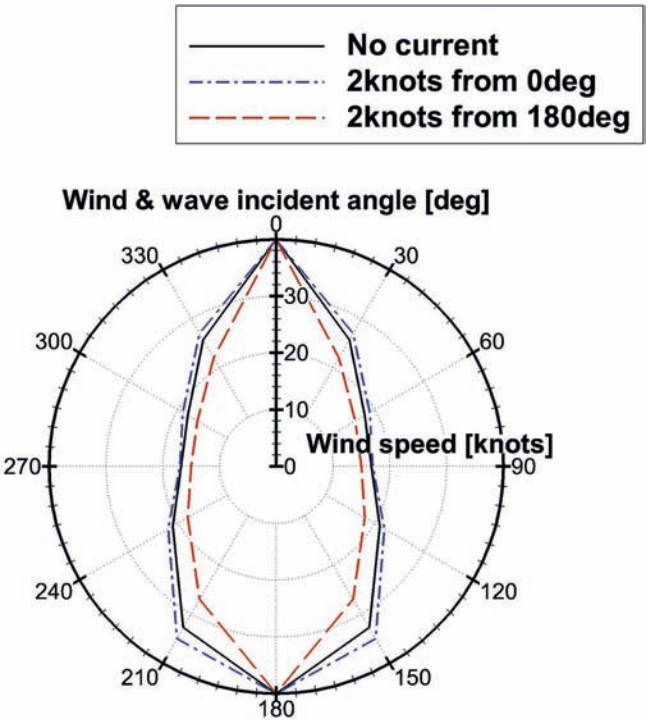

Fig. 22. Safe operation capability charts for the container ship with rudder 4 under wind, wave, and current.

from 90° to 150° and from 210° to 270° are significantly decreased. It is caused by the wave drift forces and moment since the ship is largely shifted along the transverse direction due to transversal wave loads. Rudder 1 can restrictedly meet the target wind speed assumed in Table 2 except 90° and 270°.

5. Conclusion

In this paper, we developed the concept of a safe operation capability chart which can be used as the basis of the design of a rudder by considering detailed design information such as maneuverability and environmental loads. After analysis of the predicted safe operation capability charts, two conclusions were drawn as follows.

First, a safe operation capability chart is developed from a quantified method of sailing safety. We focus on the similarity between the purposes of a DP system and an autopilot system in order to develop the safe operation capability chart. From the obtained safe operation capability charts, it is anticipated that the chart can be used as a new design approach to determine a rudder area.

Second, the applicability of the safe operation capability chart for use as the basis of design is confirmed by applying a conventional approach to determine a rudder area from IMO maneuvering tests with four different rudders. The insignificant effect of the rudder area on the mandatory tests cannot be distinguished to determining better rudder. Therefore, the rudder area must be designed empirically. Quantified capability can be used as the basis of design, because it is possible to determine the design of a rudder from parameters such as the target wind speed or target current speed, etc. As described, the suggested safe operation capability chart can be used as the basis of design as a substitute for the existing design methodology which depends on empirical judgment.

The proposed concept will be developed in two ways. First, the design of a rudder will be decided by considering the maneuvering characteristics under restricted water like the Suez Canal. Since there have been a lot of accidents that a ship collides with other vessels or walls in the Canal, the determination of a rudder area is requested to prevent the accidents. From the quantified value which indicates the safe operation capability, it is judged whether the vessel can be safely operated or not. Second, the optimum design of rudder will be confirmed by considering the predicted rudder torque. Rudder torque is the key information to prevent from enlarging a rudder area. If it is possible to design a rudder considering maneuverability and rudder torque in an early design stage, a design of a rudder can be done efficiently.

References

Andersen, O.J., Løvseth, J., 1992. The Maritime Turbulent Wind Field. Measurements and Models. Final Report for Task 4 of the Statoil Joint Industry Project. Norwegian Institute of Science and Technology, Trondheim, Norway.

Bhattacharyya, R., 1978. Dynamics of Marine Vehicles. Wiley.

DET NORSKE VERITAS (DNV), 2011. In: Recommended Practice DNV-RP-H103 (Modelling and Analyses of Marine Operation), APRIL 2011.

Fujii, J., Tsuda, T., 1961. Experimental researchs on rudder performance (2). J. Soc. Nav. Archit. Jpn. 110.

Fujii, J., Tsuda, T., 1962. Experimental researchs on rudder performance (3). J. Soc. Nav. Archit. Jpn. 111.

Fujiwara, T., Ueno, M., Nimura, T., 2001. An estimation method of wind forces and moments acting on ships. In: Mini Symposium on Prediction of Ship Manoeuvring Performance.

Germanischer Lloyd (GL), 2013. Ship Technology – PART1 Seagoing Ships – Chapter 1 Hull Structure – Section 14 Rudder and Manoeuvring Arrangement. Germanischer Lloyd (GL).

GL Noble Denton, 2010. Techniocal Policy Board Guidelines for Marine Transportations 0030/ND.

Hasegawa, K., Kouzuki, A., 1987. Automatic colli-sion avoidance system for ships using fuzzy control (in Japanese). J. Kansai Soc. Nav. Archit. 205, 1–10.

Hendzik, J., 2013. Evaluating criteria for DP vessels. J. KONES Powertrain Transp. 20 (4), 118–122.

Hwang, W., 1980. Application of System Identification to Ship Maneuvering (PhD. Thesis). Massachusetts Institute of Technology.

IACS, 1990. IACS Requirements v.1.1. S10.

IMO, 2002. MSC. 137(76) Standards for Ship Manoeuvrability. Adapted on 4 December 2002.

International Organization for Standardization (ISO) 15016, 2015. Ships and Marine Technology – Guidelines for the Assessment of Speed and Power Performance by Analysis of Speed Trial Data.

International towing tank Conference (ITTC), 2011. Prediction of Power Increase in Irregular Waves from Model Test. ITTC – Recommended Procedure 7.5-02-07-02.2.

Jung, R., 2011. Recent international development on the technical and operational measures of IMO's CO2 emission control from ships. J. Korean Soc. Mar. Environ. Eng. 14 (1), 65–71.

Kijima, K., Nakiri, Y., Tsutsui, Y., Matsunaga, M., 1990. Prediciton method of ship manoeuvrability in deep and shallow water. MARSIM ICSM 1990.

Kim, H.S., Park, G.I., Ha, M.G., 2001. Computerized measurement system of ship speed and maneuvering performance in sea trial. J. Soc. Nav. Archit. Korea 38 (3), 54–61.

Kim, Y.G., Kim, S.Y., Kim, H.T., Yu, B.S., Lee, S.W., 2006. Study on the maneuvering characteristics of a container ship with twin skegs. J. Soc. Nav. Archit. Korea 43 (1), 15–21.

Kim, Y.G., Yeo, D.J., Kim, S.Y., Yun, K.H., Oh, B.I., 2009. Prediction of maneuverability of KCS by CPMC captive model test. J. Soc. Nav. Archit. Korea 46 (6), 553–561.

Papanikolaou, A., Shigunov, V., 2014. Criteria for minimum powering and maneuverability in adverse weather conditions. In: The 14th International Ship Stability Workshop (ISSW), 29th Sep. 2014~ 1st Oct. 2014. Kuala Lumpur, Malaysia.

Papanikolaou, A., Zaraphonitis, G., Bitner-Gregersen, E., Shigunov, V., Moctar, O. El, Soares, C.G., Reddy, D.N., Sprenger, F., Energy efficient safe ship operation (SHOPERA), Influence of EEDI on Ship Design, 24–25 Sep., London, UK.

Prpic-Orsic, J., Vttor, R., Faltinsen, O.M., 2016. The influence of route choice and operating conditions on fuel consumption and CO2 emission of ships,. J. Mar. Sci. Technol. 21, 434–457.

Sung, Y.J., Park, S.H., 2015. Prediction of ship manoeuvring performance based on virtual captive model tests. J. Soc. Nav. Archit. Korea 52 (5), 407–417.

Sutulo, S., Soares, C.G., 2015. Preliminary Analysis of Ship Manoeuvrability Criteria in Wind. Maritime Technology and Engineering, London.

Sutulo, S., Soares, C.G., 2016. Analysis of Manoeuvrability Criteria and Standards in View of Environmental Factors and EEDI Impact. Maritime Technology and Engineering, London.

You, Y., Kim, W., 2016. A simplified maneuvering performance of a large container ship passing through the Suez canal. In: 4th International Conference on Ship Manoeuvring in Shallow and Confined Water with Special Focus on Ship Bottom Interaction (MASHCON). Hamburg.

You, Y., Rhee, K.P., 2016. Development of the collision ratio to infer the time at which to begin a collision avoidance of a ship. Appl. Ocean Res. 60, 164–175.

You, Y., Kim, S., Kim, W., 2017. A study on quantifying sailing safety considering maneuverability of a vessel,. J. Soc. Nav. Archit. Korea 54 (2), 113–124.